Check for updates

Modulation of room-temperature *TCR* and *MR* in La$_{1-x}$Sr$_x$MnO$_3$ polycrystalline ceramics via Sr doping

Xiaohan Yu[1] · Tao Sun[1] · Qingming Chen[1] · Yunbiao Duan[1] · Xiang Liu [1]

Abstract

La$_{1-x}$Sr$_x$MnO$_3$ (LSMO) polycrystalline samples with x content from 0.1 to 0.2 were synthesized via the optimized sol–gel method. The effect of Sr doping (x) on crystal structure, surface morphology, magnetic, and electrical transport properties of LSMO ceramics were investigated systematically. X-ray diffraction (XRD) results showed that all samples crystallized in single phases with rhombohedral structure ($R\bar{3}c$ space group), without any detectable impurity phases. With the increase of x content, lattice parameters expanded, whereas grain size of LSMO ceramic enlarged and grain boundaries (GBs) decreased accordingly. For LSMO ceramics with $x = 0.16$, peak value of temperature coefficient of resistance (TCR) reached 2.7% K^{-1} as the peak-TCR temperature (T_K) approached room temperature at 292.5 K, as well as the maximum magnetoresistance (MR) value arrived 17.9% at 300.2 K. In addition, peak TCR of LSMO ($x = 0.2$) was obtained at 6.4% K^{-1} as T_K at 329.4 K. These properties of modulation TCR and MR at room temperature in LSMO ceramics were interpreted by the interaction of double exchange mechanism and Jahn-Teller effects.

✉ Xiang Liu
   lxjim@sina.com

[1] School of Material Science and Engineering, Kunming University
    of Science and Technology, Kunming 650093 Yunnan, China

Graphical Abstract
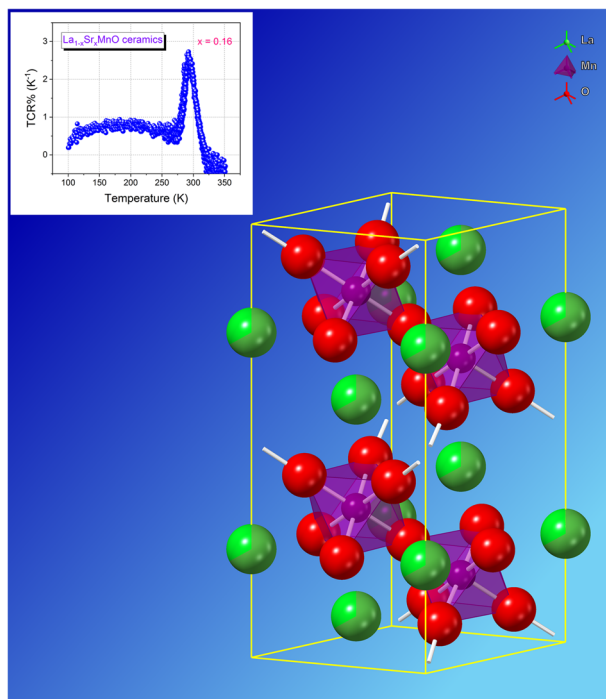
Highlights

- La$_{1-x}$Sr$_x$MnO$_3$ (0.1£ x £0.2) polycrystalline ceramics were prepared by the optimal sol-gel methods.
- Room temperature TCR and Tk of LSMO (x = 0.16) were obtained at 2.7% K-1 and 292.5 K, respectively.
- Mn^{4+} ion concentration increased by Sr doping, which was attributed to the DE and JT effects.

1 Introduction

In the past few decades, the rare-earth perovskites La$_{1-x}$A$_x$MnO$_3$, with A being Ca, Sr and Ba etc. divalent alkali element, has attracted a considerable attention due to its extraordinary magnetic and electronic properties, as well as the promise of potential applications in photo-electronic (uncooled infrared or bolometer detectors) and magnetic devices (uncooled magnetic detectors) [1–3]. In particular, fascinating colossal magnetoresistance (CMR) effect [1, 4–8], ferromagnetic (FM)-paramagnetic (PM) transition, metal-insulator (MI) transition [6], and several unusual properties, could be interpreted by the double exchange (DE) mechanism [9–12], Jahn-Teller (JT) effects [13, 14], and the grain boundaries (GBs) effect [15]. It is well known that there are two CMR effects have been found in those materials [16]. The first one is the intrinsic CMR, which was proposed by Zener in 1951 [10] and is due to DE, whereas the second one is the extrinsic CMR, which is related to the GBs and can be explained by spin-polarized tunneling [9, 17]. In addition, the

intrinsic CMR effect can be only activated at high magnetic fields of several Tesla and ultra-low temperature, which limit its application. Therefore, it is necessary to adjust the insulator-metal transition temperature (T_p) and magnetoresistance (MR) to the room temperature by changing the component in La$_{1-x}$A$_x$MnO$_3$ ceramics for the practical application. For another, the large temperature coefficient of resistance (TCR) is essential for practical applications as well [18]. The sharp drop of the resistance implies high TCR, which is useful for applications, such as temperature controlling resistance devices or bolometers detectors, etc. [9]. Unfortunately, high T_p usually corresponds to low TCR and vice versa.

For the above reasons, La$_{1-x}$Sr$_x$MnO$_3$ (LSMO) manganites have attracted extensive interests due to their large CMR and interesting room temperature physical properties. Numerous study have been focused on LSMO with the Sr content at $x = 0.33$ since an LSMO with that Sr content exhibited high-spin polarization [9], low resistivity (ρ), strong DE interaction, and a wide range of MR. However,
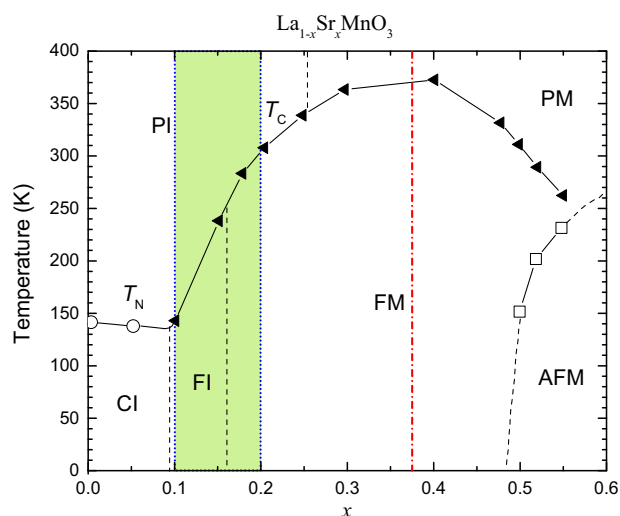
Fig. 1 The magnetic phase diagram of $La_{1-x}Sr_xMnO_3$ [4]. AFM phase is an A−type AF metal with uniform barbital order. PM, PI, FM, FI, and CI is paramagnetic metal, paramagnetic insulator, FM metal, FM insulator, and spin−canted insulator states, respectively. T_c is the Curie temperature, whereas T_N is the Neel temperature

the Curie temperature (T_C) and T_p of these manganites are still away from room temperature (295 K). In addition, these materials have low TCR and MR values, undoubtedly restricting their practical application [19, 20]. The magnetic phase diagram of LSMO is displayed in Fig. 1. It can be seen that the Curie temperature achieves the room temperature as the content of Sr varies from 0.1 to 0.2 [3, 4]. Therefore, in this work, the LSMO polycrystalline ceramics were fabricated via the optimized sol–gel method and with the Sr addition in the range of 0.1–0.2. By modulating the Sr content of the LSMO polycrystalline ceramics, the T_p and MR at room temperature were obtained. The results provide new insights into the potential applications in different fields, including uncooling bolometer and infrared detectors, magnetic sensors and magnetic recording devices at room temperature.

2 Materials and methods

A series of LSMO polycrystalline ceramics with $x = 0.1$, 0.125, 0.15, 0.16, 0.175, and 0.2 were synthesized by using the two-steps method. Compared with other methods, the sol–gel method has several advantages such as relatively homogenous size of sample granules, low temperature, and short reaction time, and so on. In this study, the relatively homogenous size of sample granules is the most important advantages to prepare high quality of LSMO polycrystalline ceramics. Firstly, LSMO powders were fabricated via the optimized sol–gel method. The solution were composed of chemical constitutions of analytical grade reagents $La(NO_3)_3$ $\cdot nH_2O$, $Mn(NO_3)_2$ aqueous solutions (50% by mass), $Sr(NO_3)_2$

and deionized water. Complexing agents including ethylene glycol and citric acid were added to the nitrate solution. Then, undergone a continuous magnetic stirring and heating, citric acid, used as polymerizing, were added to the mixture. Until the mixture became a brown gel, put it into the drying oven at 140 °C for 24 h. Secondly, after pressing at 16 MPa, the LSMO powder became the pellets and sintered at 1450 °C for 12 h under flowing oxygen at 0.02 MPa [21].

The crystal structure and surface morphology of LSMO ceramics were characterized by X-ray diffraction (XRD, ULTIMA IV) and scanning electron microscopy (SEM, SU8010), respectively. By using the conventional four-probe method in the temperature range of 100–360 K to measure the electrical and magnetic transport behaviors of the samples under an external magnetic field of 1 T with KEITHLEY Instruments.

3 Results and discussion

Figure 2a displays the XRD of the as-prepared LSMO polycrystalline samples with $x = 0.1$, 0.125, 0.15, 0.16, 0.175, and 0.2. The inset graph illustrates the enlarged views of the main peaks in the 2θ ranging from 31.6 to 33.6°. All the samples are a single phase with the crystal structure of rhombohedral phase ($R\bar{3}c$ space group). Figure 2b displays that all the samples have the (110/114) double peaks and move towards low angles with x increasing. Since the ion radius of Sr (1.26 Å) is bigger than the ion radius of La (1.16 Å), the lattice spacing of LSMO polycrystalline material increases when the content of Sr increases. Changes of the lattice parameters are listed in Table 1. Nevertheless, this substitution has not produced a modification in the crystal structure of the LSMO samples.

Figure 2c illustrates the Rietveld XRD of the $La_{0.84}Sr_{0.16}MnO_3$ ceramics. The fitting result is reported by the red line, while the diffraction data is represented by a solid sphere; green lines define the fitting diffraction peak of position, whereas the bottom line represents the difference between the fitted and the measured values. Table 1 contains the structural parameters, including space group, lattice constants (R_e, R_p, and R_b), and agreement factor (χ) describing the goodness of fit. The increment of Sr leads to an increase in the A-site ion radius, then increasing the cell volume V [22, 23]. In addition, as x increases, the a and c lattice constant also expands, which results in the change of the Mn–O bond distance ($d_{Mn–O}$) and the Mn–O–Mn bond angle ($\theta_{Mn–O–Mn}$). This could also explain why the reason the main peaks (110/104) have shifted to a lower angle. The Rietveld spectrum diffraction peak of the LSMO polycrystalline samples are in agreement with the experimental peak, which further confirms that all the samples contain a

(a)

(b)

(c)

(d)
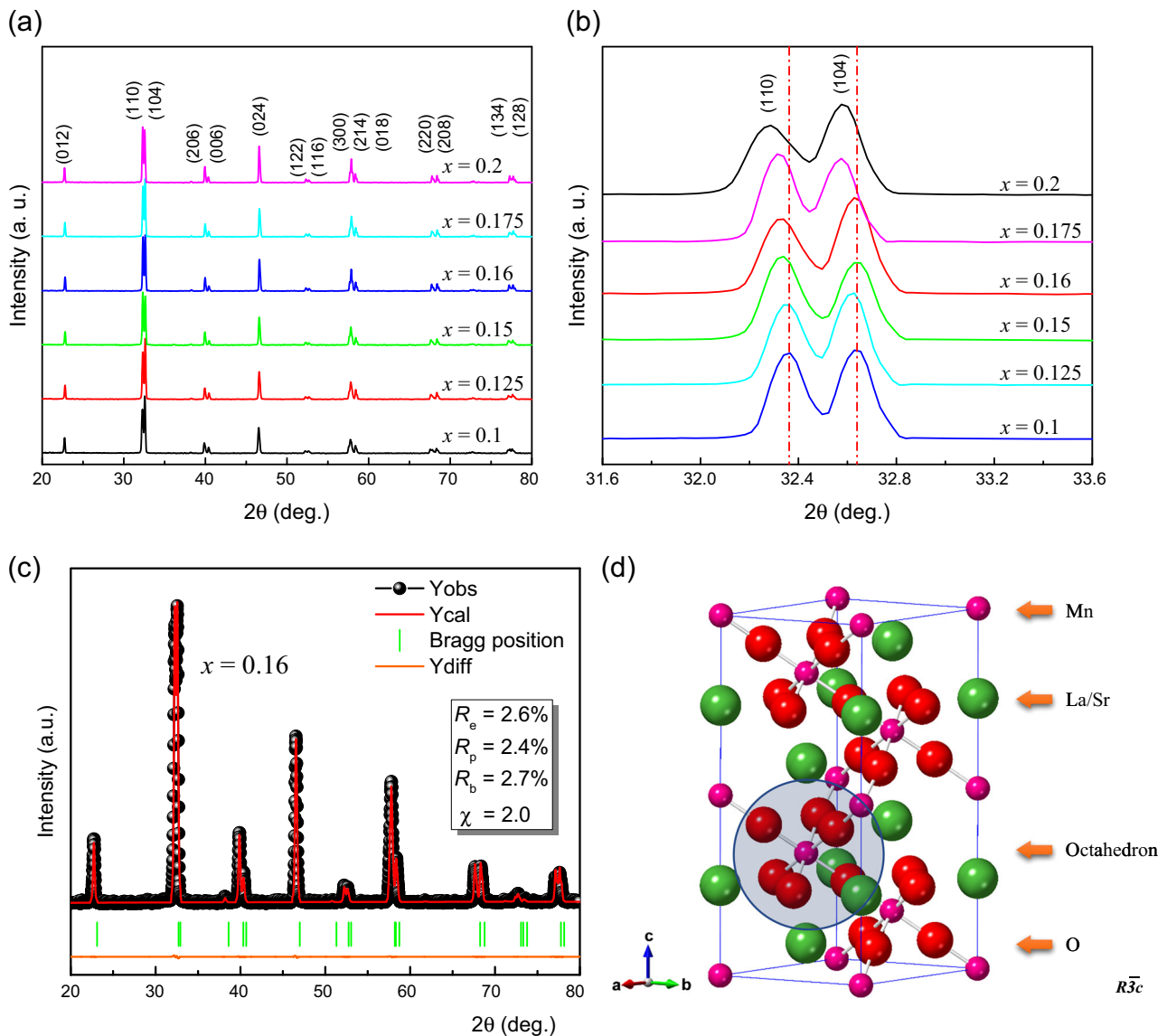
Fig. 2 a XRD patterns of LSMO with $x = 0.1$, 0.125, 0.15, 0.16, 0.175, and 0.2; **b** The enlarged views of the main peaks (110/104) in the 2θ range of 31.6–33.6°; **c** Rietveld refinement plots of the typical LSMO ($x = 0.16$) samples; **d** Typical crystal structure of $La_{1-x}Sr_xMnO_3$ ceramics

Table 1 The structure and refinement parameters of the LSMO samples

x (mol%)		0.1	0.125	0.15	0.16	0.175	0.2
Space group		$R\bar{3}c$	$R\bar{3}c$	$R\bar{3}c$	$R\bar{3}c$	$R\bar{3}c$	$R\bar{3}c$
Lattice constant (Å)	a	5.517	5.521	5.528	5.530	5.533	5.534
	c	13.360	13.362	13.365	13.366	13.369	13.370
Cell volume V (Å³)		352.15	352.81	353.75	353.8	354.44	354.60
d_{Mn-O} (Å)		1.961	1.962	1.964	1.965	1.966	1.968
$\theta_{Mn-O-Mn}$ (°)		164.532	164.534	164.540	165.541	165.543	165.632
R_e (%)		6.0	6.1	2.6	11.0	6.1	6.1
R_p (%)		6.3	6.1	2.4	6.4	6.6	6.4
R_b (%)		8.5	8.4	3.7	8.7	9.0	8.9
χ		2.0	1.9	2.0	0.6	2.2	2.1

Fig. 3 SEM images of the LSMO samples with $x = 0.1$ **a**, 0.125 **b**, 0.15 **c**, and 0.2 **d**
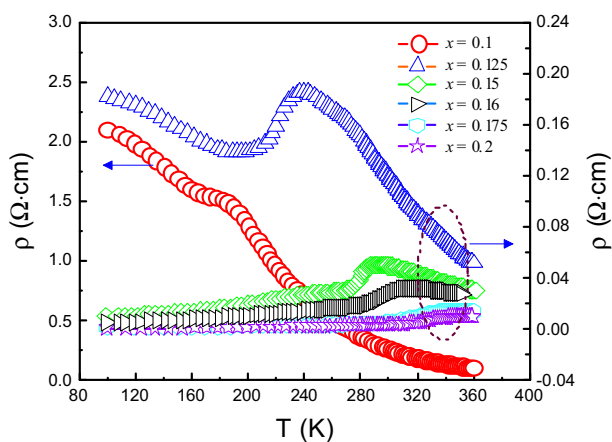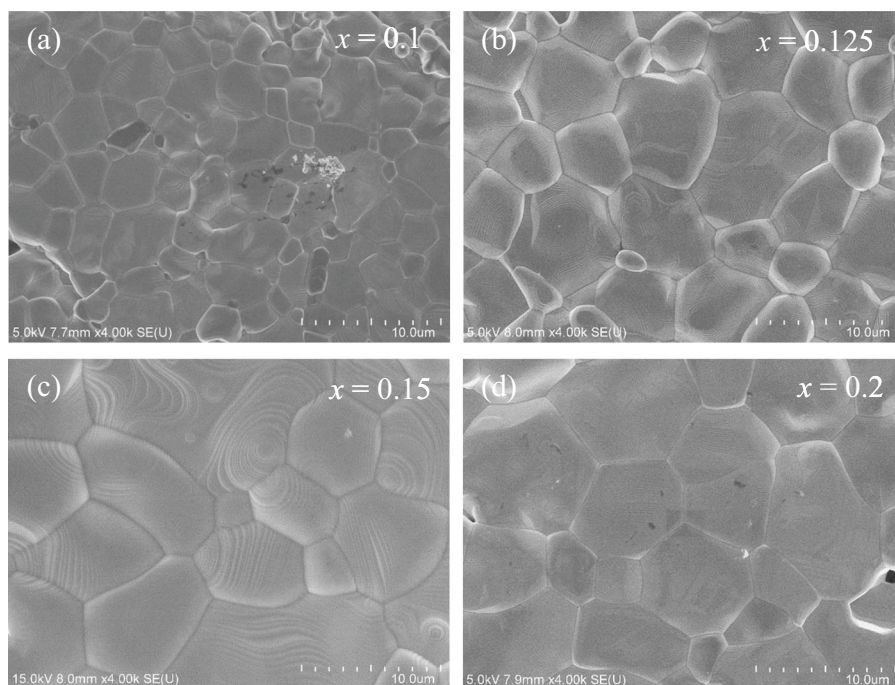
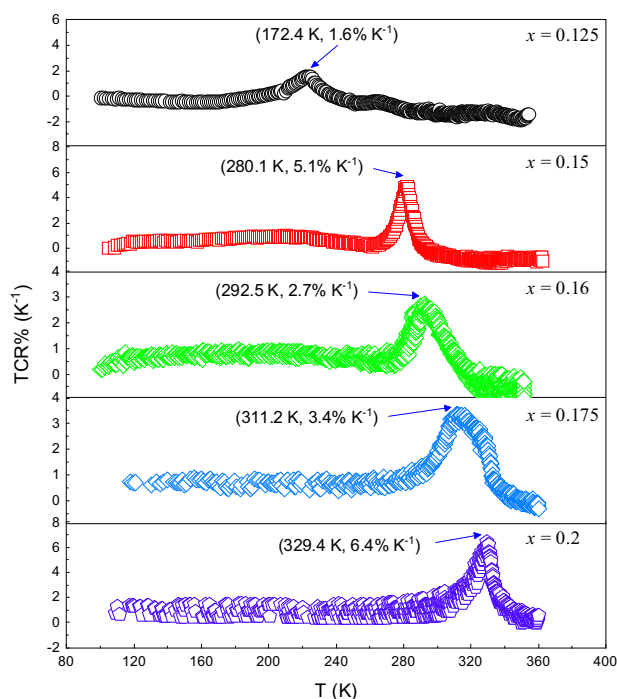**Fig. 4** Resistivity versus temperature plots of LSMO with $x = 0.1$, 0.125, 0.15, 0.16, 0.175, and 0.2

Fig. 5 *TCR* versus temperature plots of LSMO at $x = 0.125$, 0.15, 0.16, 0.175, and 0.2

single phase. Moreover, the χ value is small enough to assure the reliability of the fitting results.

The SEM micrographs of the samples are shown in Fig. 3a–d. The size of the crystalline grains varies dramatically with different Sr^{2+} doping, which means the GBs has been reduced. Indeed, the grain-size increase causes the GBs scattering to decrease, which leads to the reduction of the sample resistivity. The substitution of Ca^{2+} ion (1.12 Å) by the large Sr^{2+} ion (1.26 Å) improve the catalytic activity and promote the crystal quality of the LSMO polycrystalline samples, in turn, which degrade the quantity of GBs and increase the grain size.

Figure 4 illustrates the dependence of resistivity within a temperature range of 100–360 K for LSMO polycrystalline

material at different contents of x. With the temperature rising, all of the samples show translation from low-temperature FM to high-temperature PM insulation for both sides of T_p. Moreover, it can be seen that the resistivity (ρ) of the LSMO ceramics reduces as the content of Sr^{2+} increases. The increase of the grain sizes results in the
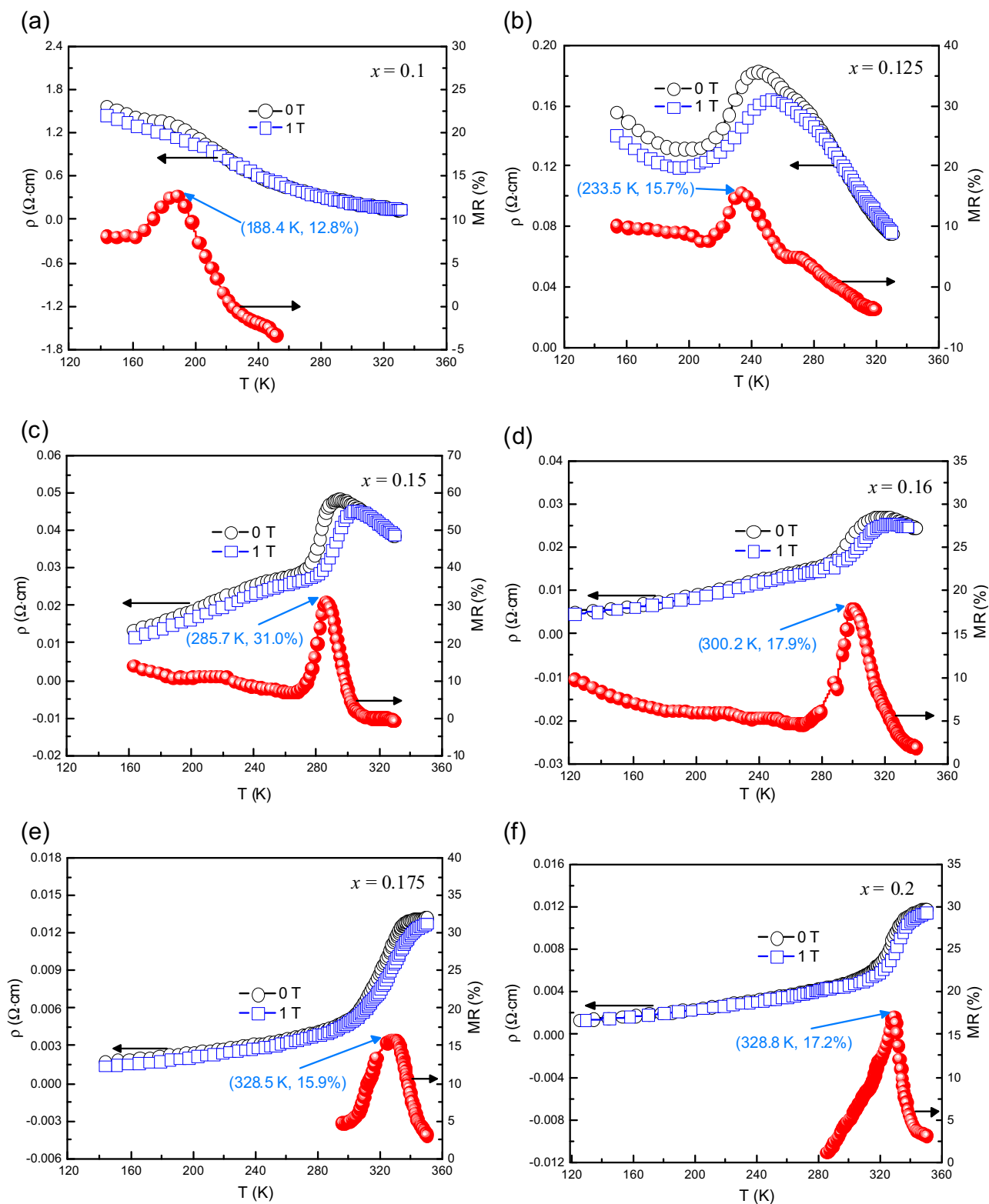
Fig. 6 ρ-T curves of the LSMO ceramics under applying external magnetic fields of 0 and 1 T, and MR versus temperature plots of LSMO with $x = 0.1$ **a**, 0.125 **b**, 0.15 **c**, 0.16 **d**, 0.175 **e**, and 0.2 **f**

decrease of the resistivity values. In previous work, it was demonstrated that several factors like doping additions,

sintering quality, and preparation method could control the grain sizes. Here, it was doping condition that is more

important in increasing the grain size of LSMO ceramics. Moreover, the T_p increased as the content of Sr^{2+}, which can be explained via the DE mechanism. The increase of Sr^{2+} ion concentration increases Mn^{4+} ion concentration inducing the changes in both Mn–O–Mn bond angles, which facilitates the DE mechanism [9].

Figure 5 displays the TCR curves of LSMO ($x = 0.125$, 0.15, 0.16, 0.175, and 0.2) ceramics, TCR defined as: TCR (%) $= [(1/\rho) \times (d\rho/dT)] \times 100\%$ [21], where T and ρ are the temperature and resistivity, respectively. As x rises, the peak TCR increases from 1.6 to 6.4%, whereas the peak-TCR temperature (T_K) values increases from 172.4 to 329.4 K. The peak TCR are 1.6%, 5.1%, 2.7%, 3.4%, and 6.4% K^{-1} for $x = 0.125$, 0.15, 0.16, 0.175, and 0.2, respectively. In addition, T_K are 172.4, 280.1, 292.5, 311.2, and 329.4 K for $x = 0.125$, 0.15, 0.16, 0.175, and 0.2, respectively. The T_K values have a similar variation trend to that of T_p. At $x = 0.16$, $T_K = 292.5$ K, approaching the room temperature, while the peak TCR reaches 2.7% K^{-1}. The peak TCR is impacted by several factors, such as ρ, tolerance factor (τ) [3], preparation method [24], and sintering quality [1], and so on. The transport point of FM–PM corresponds to the

maximum value of TCR and has great influence to the ρ, which is the most important factor to affect TCR.

Figure 6a–f shows the influence of temperature on the MR value to clarify the CMR effect. MR is defined by the following equation: MR (%) $= [(\rho_0 - \rho_H)/\rho_0] \times 100\%$ [21], where ρ_0 and ρ_H are the resistivities at the magnetic field of 0 and 1 T, respectively. From Fig. 6a–f, the ρ curves of all the samples at zero magnetic field are very close to the curves at 1 T. Furthermore, it is obvious that the value of ρ at zero is higher than the value measured under an external magnetic field of 1 T. The reason is that the external magnetic field could align the spin direction and increase the tunneling effects on the GBs to reduce resistivity [17, 25, 26]. It can be seen that the temperature of peak MR (T_M) values are 188.4, 233.5, 285.7, 300.2, 328.5, and 341.6 K for $x = 0.1$, 0.125, 0.15, 0.16, 0.175, and 0.2, respectively. Moreover, the peak MR are 12.8%, 15.7%, 31.0%, 17.9%, 15.9%, and 17.2% for $x = 0.1$, 0.125, 0.15, 0.16, 0.175, and 0.2, respectively. At $x = 0.16$ and the maximum value of MR is 17.9%, the peak MR temperature (300.2 K) approaches the room temperature.

Table 2 defined the detailed parameters for the transport properties of the LSMO ceramics. The increase of the content of Sr promotes the crystallization, which is responsible for the decrease of ρ. Moreover, the replacement of the A sites leads to a lattice distortion. Because the radius of Sr^{2+} ion is larger than the radius of La^{3+} ion, this substitution results in the τ and average radius of A sites (r_A) to increase, which lead to a stronger Mn–O–Mn exchange interaction. According to the DE theory, this interaction between Mn ions would cause a raise in T_p, T_K, and T_M. Furthermore, on the GBs, an external magnetic field could align the spin direction and increase the tunneling effects to reduce resistivity, which is the reason ρ at

Table 2 Detailed parameters for the transport properties of LSMO

Sample (x)	T_p (K)	ρ_{peak} ($\Omega \cdot cm$)	TCR (%K^{-1})	T_K (K)	MR (%)	T_M (K)
0.1	–	–	–	–	12.8	188.4
0.125	239.0	0.1854	1.6	172.4	15.7	233.5
0.15	292.1	0.0506	5.1	280.1	31.0	385.7
0.16	320.0	0.0326	2.7	292.5	17.9	300.2
0.175	351.0	0.0139	3.4	311.2	15.9	328.5
0.2	358.6	0.0102	6.4	329.4	17.2	341.6

Table 3 The peak TCR (%) and MR (%) obtained in previous and this work

Sample	Peak TCR% (K^{-1})	Peak TCR% temperature (K)	Peak MR (%)	Peak MR temperature (K)	Magnetic field (T)	References
$La_{0.7}Sr_{0.3}MnO_3$	3.4	~180	17	~380	1.0	[20]
$La_{0.67}Sr_{0.33}MnO_3$	3.4	325	–	–	–	[27]
$La_{0.67}Sr_{0.33}MnO_3$	2.1	361	–	–	–	[28]
$La_{0.7}Sr_{0.3}MnO_3$	1.8	~370	32	370	7.0	[1]
$La_{0.7}Ba_{0.3}MnO_3$	0.4	~320	39	332	7.0	[1]
$La_{0.7}Ba_{0.3}MnO_3$: $Ag_{0.3}$	1.8	~300	–	–	–	[1]
$La_{0.7}Ca_{0.3}MnO_3$	1.5	~260	59	266	7.0	[1]
$La_{0.7}Sr_{0.3}MnO_3$: $Ag_{0.4}$	2.2	~350	34	~365	7.0	[1]
$La_{0.65}Sr_{0.35}MnO_3$	0.9	~85	–	–	–	[29]
$La_{0.84}Sr_{0.16}MnO_3$	2.7	292.5	17.9	300.2	1.0	This work
$La_{0.8}Sr_{0.2}MnO_3$	6.4	329.4	17.2	328.8	1.0	This work

1 T is lower than that at zero. In addition, many other factors can influence the TCR, such as sintering time, temperature, r_A, τ, preparation method, and resistivity of samples.

Table 3 shows the obtained TCR and MR peak in comparison with reported values. In previous work, the peak TCR were 3.4% K^{-1} in LSMO ($x = 0.33$) ceramics. However, the peak TCR temperature (325 K) was above the room temperature, a condition that limits its application. However, in this work, we obtained the peak TCR (2.7% K^{-1}) with T_K at 292.5 K for $x = 0.16$, as well as the maximum MR (17.9%) at 300.2 K. Furthermore, the peak TCR (6.4% K^{-1}) in the $La_{0.8}Sr_{0.2}MnO_3$ polycrystalline ceramics is significantly larger than other previous reports [1, 27–29]. Our findings suggest that the $La_{0.84}Sr_{0.16}MnO_3$ ceramics have broad applications prospects in the room temperature uncooled infrared Bolometer and magnetic devices.

4 Conclusions

The LSMO polycrystalline ceramics with $x = 0.1$, 0.125, 0.15, 0.16, 0.175, and 0.2 were prepared via the optimal sol–gel methods. XRD showed all the bulk samples crystallized in single phase and with the crystal structure of rhombohedral phase ($R\bar{3}c$ space group). As the x content increased, the main diffraction peaks (110/114) of XRD shifted downwards to low angles, increasing the lattice structure parameters (a, c, and V) of the LSMO ceramics as well. This was attributed to the Sr ion radius (1.26 Å) being bigger than the La ion radius (1.16 Å) at the A sites. In addition, with x content further increased, T_p increased gradually, while the peak value of TCR fluctuated and reached a maximum value. By applying an external magnetic field of 1 T, the resistivity of the LSMO ceramics was lower than the samples without the magnetic field, which could be interpreted by spin-polarized tunneling occurring with the function of spin disorder in the GBs. For the sample of $x = 0.16$, the peak values of TCR and MR attained 2.7% K^{-1} (292.5 K) and 17.9% (300.2 K), respectively. At the same time, the large peak TCR was observed with the highest value of 6.4% K^{-1} at 329.4 K for the LSMO ($x = 0.2$) sample. These properties were related to DE mechanism and JT effects, which suggested that the LSMO ceramics ($x = 0.16$) may have underlying applications in uncooling infrared detectors or bolometers, magnetic sensors, and magnetic recording devices at room temperature.

Compliance with ethical standards

Conflict of interest The authors declare that they have no conflict of interest.

Publisher's note: Springer Nature remains neutral with regard to jurisdictional claims in published maps and institutional affiliations.

References

1. Tripathi R (2008) Search for room temperature high-TCR manganite/silver composites. J Magn Magn Mater 320:L89–L92. https://doi.org/10.1016/j.jmmm.2008.01.039

2. Bhatt RC, Srivastava PC, Agarwal SK, Awana VPS (2013) Observance of improved magneto-resistance and magnetic entropy change in $La_{0.7}(Ca_{0.2}Sr_{0.1})MnO_3$:Pd composite. J Supercond Nov Magn 27:1491–1497. https://doi.org/10.1007/s10948-013-2462-3

3. Zhao S, Yue X, Liu X (2017) Tuning room temperature Tp and MR of $La_{1-y}(Ca_{y-x}Sr_x)MnO_3$ polycrystalline ceramics by Sr doping. Ceram Int 43:4594–4598. https://doi.org/10.1016/j.ceramint.2016.12.121

4. Dagotto E, Hotta T, Moreo A (2001) Colossal magnetoresistant materials: the key role of phase separation. Phys Rep 344:1–153. https://doi.org/10.1016/S0370-1573(00)00121-6

5. Haghiri-Gosnet A-M, Renard J-P (2003) CMR manganites: physics, thin films and devices. J Phys D: Appl Phys 36:R127–R150. https://doi.org/10.1088/0022-3727/36/8/201

6. Ramakrishnan TV (2007) Modelling colossal magnetoresistance manganites. J Phys: Condens Matter 19:125211. https://doi.org/10.1088/0953-8984/19/12/125211

7. Goodenough JB (1997) Electronic structure of CMR manganites. J Appl Phys 81:5330–5335. https://doi.org/10.1063/1.364536

8. Helmolt RV, Wecker J, Holzapfel B, Schultz L, Samwer K (1993) Giant negative magnetoresistance in perovskitelike LBMO ferromagnetic films. Phys Rev Lett 71:2331–2333. https://doi.org/10.1103/PhysRevLett.71.2331

9. Jin F, Zhang H, Chen Q (2018) Improved Curie temperature and temperature coefficient of resistance (TCR) in $La_{0.7}Ca_{0.3-x}Sr_xMnO_3$:$Ag_{0.2}$ composites. J Alloy Compd 747:1027–1032. https://doi.org/10.1016/j.jallcom.2018.03.117

10. Jahn HA, Teller E (1937) Stability of polyatomic molecules in degenerate electronic states. I. Orbital degeneracy. Proc R Soc A 161:220–235. https://doi.org/10.1098/rspa.1937.0142

11. Li DG, Mai YT, Xoing J, Xiong YH, Liu ZL, Xiong CS (2012) Studies on low-field and room-temperature magnetoresistance in $La_{2/3}(Ca_{1-x}Sr_x)_{1/3}MnO_3$ Perovskites. J Supercond Nov Magn 26:719–723. https://doi.org/10.1007/s10948-012-1798-4

12. Thanh TD, Nguyen LH, Manh DH, Chien NV, Phong PT, Khiem NV, Hong LV, Phuc NX (2012) Structural, magnetic and magnetotransport behavior of $La_{0.7}Sr_xCa_{0.3-x}MnO_3$ compounds. Phys B: Condens Matter 407:145–152. https://doi.org/10.1016/j.physb.2011.10.006

13. Zener C (1951) Interaction between the d-shells in the transition metals. II. Ferromagnetic compounds of manganese with Perovskite structure. Phys Rev 82:403–405. https://doi.org/10.1103/PhysRev.82.403

14. Millis AJ, Littlewood PB, Shraiman BI (1995) Double exchange alone does not explain the resistivity of $La_{1-x}Sr_xMnO_3$. Phys Rev Lett 74:5144–5147. https://doi.org/10.1103/PhysRevLett.74.5144

15. Kuberkar DG, Doshi RR, Solanki PS, Khachar U, Vagadia M, Ravalia A, Ganesan V (2012) Grain morphology and size disorder effect on the transport and magnetotransport in sol–gel grown

nanostructured manganites. Appl Surf Sci 258:9041–9046. https://doi.org/10.1016/j.apsusc.2012.05.149

16. Dhahri A, Jemmali M, Dhahri E, Hlil EK (2015) Electrical transport and giant magnetoresistance in $La_{0.75}Sr_{0.25}Mn_{1-x}Cr_xO_3$ (0.15, 0.20 and 0.25) manganite oxide. Dalton Trans 44:5620–5627. https://doi.org/10.1039/c4dt03662j

17. Kresse G, Hafner J (1994) Ab initiomolecular-dynamics simulation of the liquid-metal–amorphous-semiconductor transition in germanium. Phys Rev B 49:14251–14269. https://doi.org/10.1103/PhysRevB.49.14251

18. Liu X, Yan YZ, Chen QM, Zhang H, Cao MG, Zhang SC, Zhang PX (2013) High TCR (temperature coefficient of resistance) $La_{2/3}Ca_{1/3}MnO_3$:Ag_x polycrystalline composites. Appl Surf Sci 283:851–855. https://doi.org/10.1016/j.apsusc.2013.07.032

19. Awana VPS, Tripathi R, Balamurugan S, Kishan H, Takayama-muromachi E (2006) Magneto-transport of high TCR (temperature coefficient of resistance) $La_{2/3}Ca_{1/3}MnO_3$:Ag polycrystalline composites. Solid State Commun 140(9–10):410–415. https://doi.org/10.1016/j.ssc.2006.09.021

20. Vadnala S, Durga Rao T, Pal P, Asthana S (2014) Study of structural effect on Eu-substituted LSMO manganite for high temperature coefficient of resistance. Phys B 448:277–280. https://doi.org/10.1016/j.physb.2014.04.029

21. Sun T, Zhao S, Ji F, Liu X (2018) Enhanced room-temperature MR and TCR in polycrystalline $La_{0.67}(Ca_{0.33-x}Sr_x)MnO_3$ ceramics by oxygen assisted sintering. Ceram Int 44:2400–2406. https://doi.org/10.1016/j.ceramint.2017.10.209

22. Yang W, Wang L, Lin J, Li X, Xiu H, Shen Y (2016) Effect of A site and oxygen vacancies on the structural and electronic properties of lead-free $K Ta_{0.5}Nb_{0.5}O_3$ crystal. J Electron Mater 45:3726–3733. https://doi.org/10.1007/s11664-016-4477-6

23. Venkataiah G, Prasad V, Venugopalreddy P (2007) Influence of A-site cation mismatch on structural, magnetic and electrical properties of lanthanum manganites. J Alloy Compd 429:1–9. https://doi.org/10.1016/j.jallcom.2006.03.081

24. Yin X, Liu X, Yan Y, Chen Q (2014) Preparation of $La_{0.67}Ca_{0.33}MnO_3$:Ag_x polycrystalline by sol–gel method. J Sol-gel Sci Techn 70:361–365. https://doi.org/10.1007/s10971-014-3290-z

25. Blöchl PE (1994) Projector augmented-wave method. Phys Rev B 50:17953–17979. https://doi.org/10.1103/PhysRevB.50.17953

26. Venkataiah G, Huang JCA, Reddy PV (2010) Low temperature resistivity minimum and its correlation with magnetoresistance in $La_{0.67}Ba_{0.33}MnO_3$ nanomanganites. J Magn Magn Mater 322:417–423

27. Chromik Š, Štrbík V, Dobročka E, Roch T, Rosová A, Španková M, Lalinský T, Vanko G, Lobotka P, Ralbovský M, Choleva P (2014) LSMO thin films with high metal–insulator transition temperature on buffered SOI substrates for uncooled microbolometers. Appl Surf Sci 312:30–33. https://doi.org/10.1016/j.apsusc.2014.05.051

28. Zhao S, Yue X-J, Yan Y-Z, Liu X (2016) Effects of Ag addition on the structural and electrical properties of $La_{0.67}Sr_{0.33}MnO_3$ ceramics. Adv Appl Ceram 116:180–184. https://doi.org/10.1080/17436753.2016.1265755

29. Kagomiya I, Matsumoto S, Kakimoto K-i, Ohsato H, Sakai H, Maeda Y (2009) Controlling temperature coefficient of resistivity in $La_{1-x}Sr_xMnO_3$ ceramics. Mater Lett 63:2452–2455. https://doi.org/10.1016/j.matlet.2009.08.032